Compressive Strength of Iron-Ore Agglomerates

M.A. Meyers and P.P. Meyers

Abstract—*The analysis of the phenomena involved in determining the compressive strength of iron-ore agglomerates leads to the identification of important parameters. It is shown mathematically that the pellet rupture strength is proportional to the cross-sectional area. Fracture is initiated at the center of the pellets by the tensile stresses developed by the compressive loads normally to the compressive axis. The variation in strength between individual pellets of identical composition and subjected to identical treatments is due to internal voids of varying sizes that act as stress-concentration sites.*

Two novel testing procedures are proposed. The first consists of testing the pellets between two plates having three steel spheres each. This configuration simulates much better the environment actually encountered by the pellets. The second procedure consists of a thick-walled cylinder in which a piston penetrates; a large group of pellets is tested simultaneously, as the stress versus strain plot is being recorded. This latter test presents significant advantages over the conventional testing procedure; the main one is that one single test is sufficient to characterize the mechanical response of the pellets.

Introduction

The objectives of the investigation were to establish a scientific understanding of the phenomena involved in the fracture of pellets and of the important parameters, and, based on it, to propose an improved testing technique.

The compression test routinely applied on pellets is addressed. A mathematical analysis is conducted to correlate pellet strength to dimensions. The fracture surfaces are analyzed and the rupture phenomenon is interpreted in terms of the fracture morphology and stress state set up in the pellets. The causes for variation in strength are analyzed.

Two novel testing procedures are described; their advantages and disadvantages with respect to the accepted test are discussed.

Conventional Test

Mathematical Analysis

The only theoretical treatment dealing with compression of agglomerates is, to the authors' knowledge, that by Kapur and Fuerstenau (1967). They analysed the failure in limestone agglomerates and attributed fracture to the formation of shear cones at the top and bottom.

An alternative explanation is that fracture is produced by the tensile stresses set up by the compressive loads acting along directions normal to the loading axis. These stresses are highest at the center of the sphere.

Figure 1 depicts the formation of a fracture in the central region due to the tensile stresses when a sphere is compressed. This phenomenon is not unique to pellets. Indeed, steel cylinders undergo a "central burst" due to tensile stresses when compressed (Dieter, 1976). This is actually the principle used in the Mannesmann tube-piercing process (McGannon, 1970). And Jaeger and Cook (1979) report that cylindrical or disk-shaped rock specimens fail by the tensile stresses set up at the center. The mathematical analysis that follows is based on a similar derivation conducted by Timoshenko (1934) for a disk. The extension of the solution to an axisymmetric problem is described below.

Figure 2 shows a sphere being compressed between two parallel platens (load P). At the point of contact, the stress would be infinite if the sphere and platen are rigid. This problem has been treated by Hertz (1896) and the stresses are called Hertzian stresses. It will be shown that these stresses are not important in the fracture process. The analysis presented does not consider the Hertzian stresses at the sphere-plate contact surface.

Following the procedure of Timoshenko (1934), it is assumed that each of the forces produces a simple radial stress distribution at the surface of the sphere. In order to understand the derivation below, the reader should consult Timoshenko (1934). For this, the force P is replaced by a force distribution $f(\theta)$ that, integrated over the whole surface of the platen, provides P.

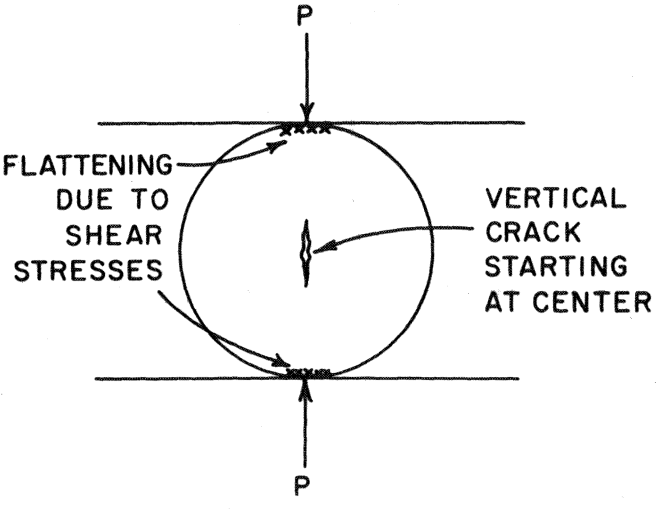

Fig. 1—Schematic drawing showing sphere compressed between platens and fracture being produced by tensile stresses set up at center

$$\int_0^{\pi/2} f(\theta) \cos\theta \, d\theta = P \tag{1}$$

If one makes

$$f(\theta) = \frac{4 P \cos\theta}{\pi} \tag{2}$$

one can satisfy Equation 1. A cone with an apex at the sphere-platen interface intersects the sphere along a circle. A disk is defined at this circle and the stress distribution acting on it is balanced by the distributed force acting on the platen. The stress is shown as σ_r in Fig. 2. One can write the equilibrium-of-forces equation

$$\sigma_r \, r \, d\theta \, L = f(\theta) \, d\theta \tag{3}$$

L is the length of the circle in the disk:

$$L = 2\pi r_2 = 2\pi r \sin\theta \tag{4}$$

M.A. Meyers is an associate professor in the Department of Metallurgical and Materials Engineering, New Mexico Institute of Mining and Technology, Socorro, NM, and **P.P. Meyers** is manager, sales division, Ferteco Mineracao, Rio de Janeriro, RJ, Brazil. SME preprint 81-302. SME-AIME Fall Meeting, Denver, CO, November 1981. Manuscript May 1981. Discussion of this paper must be submitted, in duplicate, prior to Aug. 31, 1984.

Hence:

$$r = \frac{2\,P\cos\theta}{\pi^2 r_1^2 \sin\theta_1} \tag{5}$$

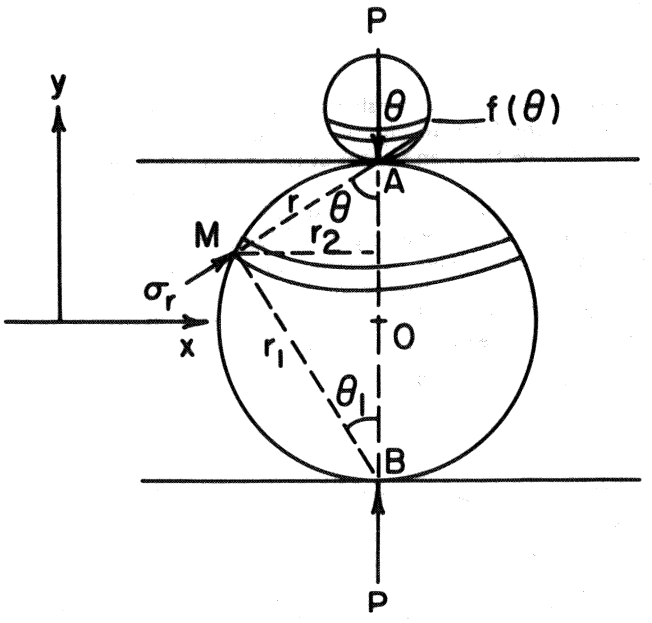

Fig. 2—Force P acting on pellet being replaced by distributed force f(θ) which generates radial stress distribution. At point M, one has σ_r

Similarly, if one considers the force P acting in the lower platen, at a distance r_1 from M, one can write:

$$\sigma_{r_1} = \frac{2\,P\cos\theta_1}{\pi^2 r_1^2 \sin\theta_1} \tag{6}$$

r and r_1 are perpendicular due to the geometry. It will be shown that σ_r is equal to σ_{r1}; applying the relations (d is the sphere diameter)

$$\cos\theta = \frac{r}{d} \text{ and } \frac{\cos\theta}{r} = \frac{1}{d}$$

$$\sin\theta = \frac{r_1}{d} \text{ and } r\sin\theta = \frac{rr_1}{d}$$

to Equations 5 and 6, one obtains:

$$\sigma_r = \sigma_{r_1} = \frac{2P}{\pi^2 r r_1} \tag{7}$$

The product rr_1 is a constant along circles that are parallel to the platens. This allows the continuation of the same derivation procedure as the one adopted by Timoshenko. The calculations that follow apply to one circle. The horizontal and vertical components of the stresses acting on each point of the surface of the sphere can be obtained by taking the projection of σ_r and σ_{r1} on the xx and yy axes, respectively. Equation 63 of Timoshenko presents them (there is a mistake; σ_x should read σ_y and vice-versa). They can be obtained by applying Equations 2.5 and 2.6 of Dieter (1976):

$$\sigma_x' = \frac{\sigma_r}{2} - \frac{\sigma_r}{2}\cos 2\theta$$

$$\sigma_x' = \frac{\sigma_r}{2}(1-\cos 2\theta) = \sigma_r \sin^2\theta \tag{8}$$

$$\sigma_y' = \frac{\sigma_r}{2} + \frac{\sigma_r}{2}\cos 2\theta = \sigma_r \cos^2\theta \tag{9}$$

To calculate the total stress acting on a point of the sphere one has to consider the external forces (except for the contact points). At each point M on the surface, a tensile stress ($-\sigma_r$) has to be added to σ_x and σ_y:

$$\sigma_x = -2\,\sigma_{r_1}\sin^2\theta + \sigma_r = \frac{2P}{\pi^2 r r_1}\,(1-2\sin^2\theta) \tag{10}$$

$$\sigma_y = -2\sigma_r\cos^2\theta + \sigma_r = \frac{2P}{\pi^2 r r_1}\,(1-2\cos^2\theta) \tag{11}$$

Equations 10 and 11 satisfy the boundary conditions. For instance, when point M is at the diametral surface along the midplane of the sphere, $\theta = \theta_1 = \pi/2$ and $\sigma_x = \sigma_y = 0$. The normal stress is zero at the free surface. The values of σ_x and σ_y along the diametral plane parallel to the platens can be expressed ($r = r_1$) from Equation 10 and 11:

$$\sigma_x = \frac{2P}{\pi^2}\left(x^2 + \frac{d^2}{4}\right)^{-1}\left[1 - 2x^2\left(x^2 + \frac{d^2}{4}\right)^{-1}\right] \tag{12}$$

$$\sigma_y = \frac{2P}{\pi^2}\left(x^2 + \frac{d^2}{4}\right)^{-1}\left[1 - \frac{d^2}{2}\left(x^2 + \frac{d^2}{4}\right)^{-1}\right] \tag{13}$$

σ_x has its maximum value at the center of the sphere. By making x = 0 in Equation 12, one finds:

$$(\sigma_x)_{x=0} = \frac{8\,P}{\pi^2 d^2} \tag{14}$$

The minimum for σ_y is, similarly, at the diametral plane, reached when x = 0 in Equation 13:

$$(\sigma_y)_{x=0} = -\frac{8\,P}{\pi^2 d^2} \tag{15}$$

More complex computations have been conducted by Sternberg and Rosenthal (1952), among others. They arrive at equations fairly similar to Equation 14. Figure 3 shows the variation of σ_x and σ_y along the diametral plane.

Equation 15 can be converted into an expression giving the strength of the pellet. If one assumes that the pellet breaks when the tensile stress reaches a critical level σ_c, then:

$$P_c = \frac{\pi^2 d^2 \sigma_c}{8} \tag{16}$$

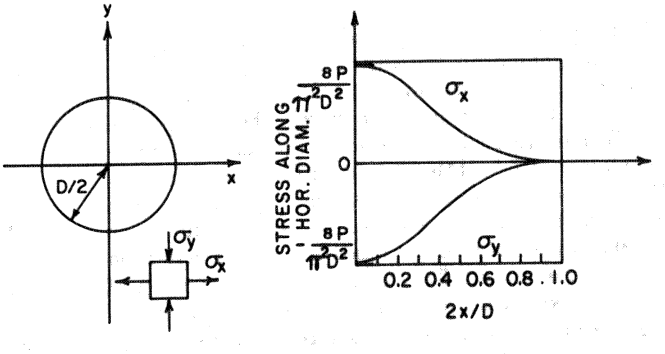

Fig. 3—Stresses as a function of distance from center along diametral plane perpendicular to loading direction; σ_x' tensile, σ_y' compressive

If σ_c is a characteristic parameter of the material, then the rupture load P_c should increase with the cross-sectional area. The slope of a P_c versus $\pi d^2/4$ plot provides the tensile strength of the pellet ($\sigma_c/2$). Assuming that the maximum normal stress criterion (Rankine criterion) holds, the normal compressive stress σ_y should not have an effect on the failure stress, σ_c. This is a reasonable assumption for brittle materials (Popov 1976). The same principle is used in the "Brazilian" test commonly applied to rocks: a compressive test yields the tensile strength.

Compression Test on Pellets

A number of compressive tests were conducted on iron ore pellets obtained from the Samarco pelletizing plant in Ponta Ubu, Brazil. These pellets are formed by disk pelletizing a hematite iron ore, (particle size less than 50 μm) water, and lime mixture. They are hardened in a traveling-grate furnace and the nominal diameter varies 9-16 mm (0.3-0.6 in.)

The pellets were tested at ambient temperature in a Tinius-Olsen and in a Riehle universal testing machine. A cross-head velocity lower than the one recommended by I.S.O. (1974) was chosen to allow for a greater ability to control the test parameters. The fracture occurred most often along a vertical plane. The sphere was divided into two or more parts by the fracturing process.

Figure 4 shows a top view of fracture pellets, that were divided into two and three parts. A closer observation of the fracture surface with a scanning-electron microscope revealed features that definitely establish the fracture process as a tensile cleavage-type (Fig. 5). The fracture is transgranular: it goes through the original hematite particles that are smaller than 50 μm. These individual particles can be seen very clearly.

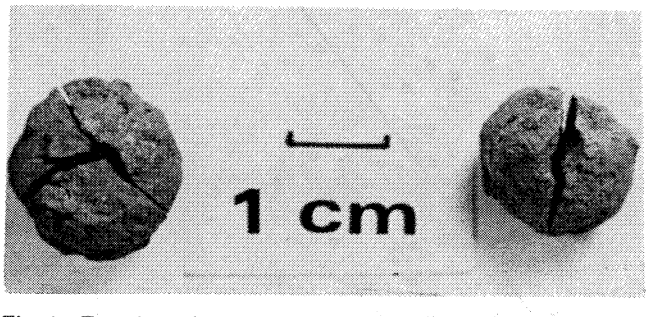

Fig. 4—Top view of typical fractured pellet; fracture planes perpendicular to plane of platens

The fracture surface in the region between the particles is not as smooth as inside the particles. This shows that the fracture is indeed transgranular and that the interface region has the same or greater tensile strength than the hematite particles.

The region immediately adjoining the platen-pellet contact has a completely different morphology. On visual observation, it exhibited a redish coloration, in contrast with the metallic luster exhibited by the cleavage region, which consists of about 98% of the fracture surface. Scanning electron microscopy confirms the completely different morphology indicative of a different operating fracture mechanism.

Figure 6a shows a flat portion corresponding to the contact surface of the pellet and a more irregular region adjoining it. This irregular region is magnified in Fig. 6b. In contrast with Fig. 5b, the particles are much smaller and more irregular. Their size is around 5 μm. Hence, the original hematite particles are crushed. This feature is clearly indicative of shear failure. The extremely high compressive stresses set up at the contact region generate, at 45°, shear stresses that fracture the hematite particles.

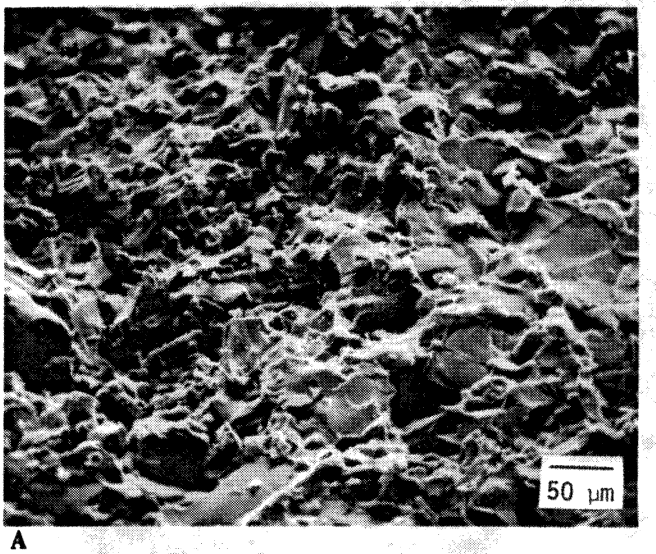

A

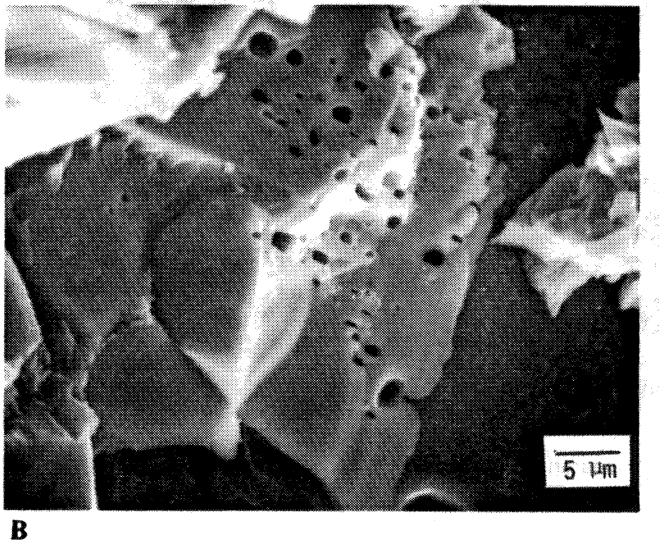

B

Fig. 5—Appearance of fracture "cleavage" region

The existence of such a shear failure region has been recognized by Jaeger and Cook (1979) and Kapur and Fuerstenau (1967). Jaeger and Cook do not attribute any importance to it in establishing the complete fracture. It can be concluded that the fracture of the pellets is indeed caused by tensile stresses, that are maximum at the center.

Figure 7a shows a first attempt at correlating the pellet dimension with fracture strength in accord with Equation 16 derived in the preceding section. The pellet cross-sectional area was obtained by computing it from its weight, assuming a sphere. The density was obtained by measuring the diameter of pellets that were hand-ground in order to render them more spherical. It was found to be 3.83 t/m^3 (3.83 g/cm^3).

The first observation that can be made is that the scatter in the data is very large. There are several possible causes for this pellet irregularity, existence of internal voids, intrinsic variations in strength, and size.

In spite of the wide scatter, a least-squares fit shows a tendency towards greater strength with greater cross-sectional area. The line intersects the load axis at 700 N (157 lbf). Kapur and Fuerstenau (1967), on the other hand, plotted the pellet strength (limestone pellets) versus the mass, and fitted the relationship into a straight line.

In order to extend the range of pellet size beyond the one available and verify whether surface imperfections might be responsible for the variation in strength, pellets were polished in a rotating disk with sandpaper prior to testing. Figure 7b shows the results and the P versus d^2 correlation is much clearer, especially at small sizes.

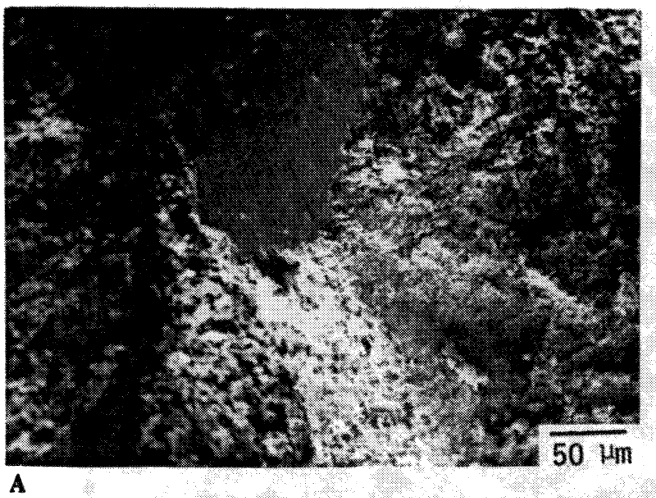

A

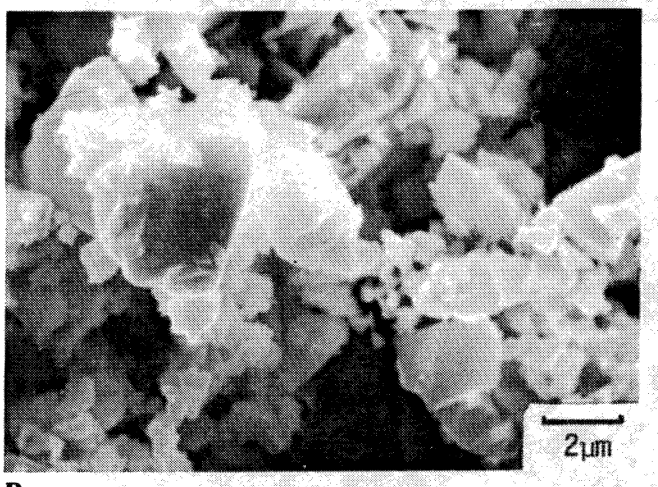

B

Fig. 6—Appearance of fracture close to pellet-platen contact region

Polishing the surface does not have a noticeable effect on the variation of strength and it is concluded that there is an intrinsic strength variation between individual pellets. The intercept of the least-square-fit line is 265 N (59.5 lbf), and the standard deviation of this intercept is 340 N (76.4 lbf). One can safely say that the line passes through the origin. By applying Equation 16 it is possible to calculate the tensile strength of the pellets, σ_c. The slope of the line in Fig. 7 (P/A) is equal to $\pi\sigma_c/2$. A value of $\sigma_c = 18.5\ MN/m^2$ is found.

In order to distinguish between fracture produced by the mechanism proposed herein and fracture proposed by Kapur and Fuerstenau's mechanism, padded tests were performed. Two small rubber pads were glued to each pellet so that the direct contact between the pellet and the platen was avoided during the compression test. In this manner, the formation of the crushed cone region was retarded or completely eliminated. Thirty padded and 30 conventional pellets, with diameters between 9.5-12.7 mm (0.4-0.5 in.) were tested. The padded pellets exhibited a mean strength of 4.7 kN (0.5 tonf), with a standard deviation of 1.6 kN (0.2 tonf), the unpadded pellets exhibited a mean strength of 4 kN (0.4 tonf) with a standard deviation at 1.2 kN (0.1 tonf). The slightly higher strength of the padded pellets indicates that the formation of the crushed cone might have an effect on the fracture. However, the main fracture mode seems to be the one determined by the tensile stresses.

In an attempt to investigate the effects of internal voids on the strength of pellets, diametral cuts were made on two pellets with a diamond saw (Isomet). The composite photograph obtained by scanning electron microscopy operating at the minimum magnification is shown in Fig. 8.

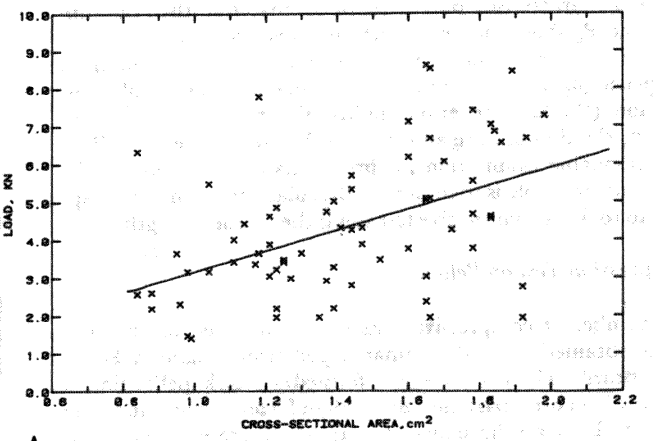

A

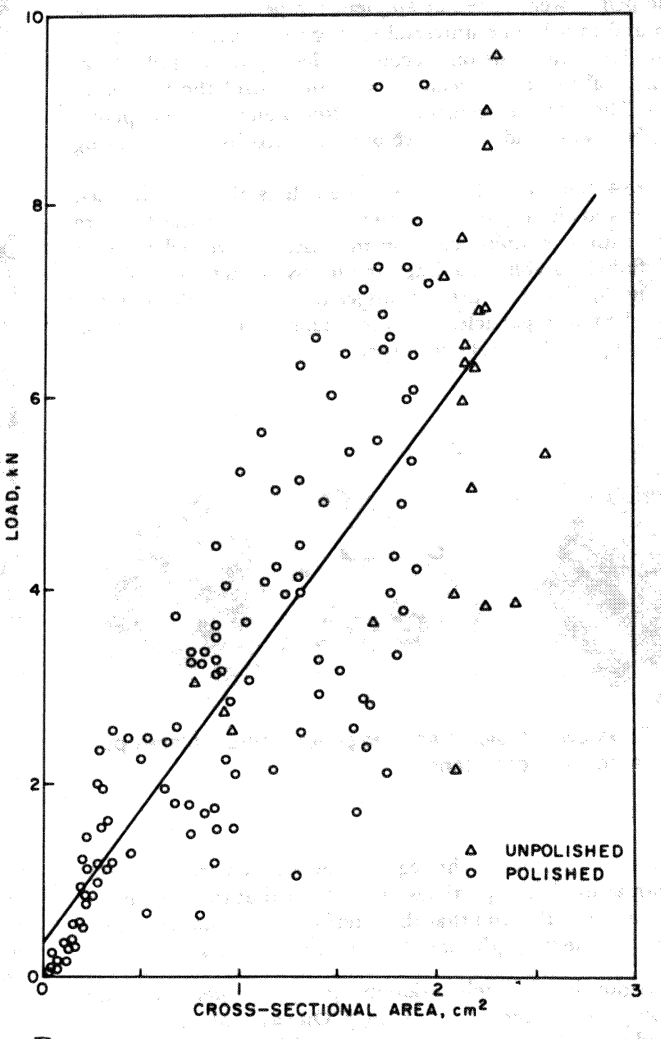

B

Fig. 7—Fracture load, P_C, versus cross-sectional area of pellets, using conventional test; straight line represents least-square fit

The significant density of voids vary in size from 0-0.3 mm (0.012 in.). The large porosity exhibited by the pellets is due to the fact that they are not compacted or densified and water is trapped between the particles in the green pellets, later expelled during the sintering process.

The density of the voids was measured at a magnification of 22 x using the Spektor's method described by de Hoff and Rhines (1968). The voids are assumed to be spherical and the chord length is measured by the intercept method. The total length of lines on which measurements were made was 900 mm (35 in.) and 1,300 voids were counted.

Figure 9 shows the densities of voids in the different size groups. The void sizes below about 0.04 mm (0.0015 in.) cannot be seen at the magnification in which the measurements were made so they are not included in the plot. The presence of these voids can have a profound effect on the mechanical strength of the pellets.

In fracture mechanics, the effect of flaws on the mechanical properties of materials is studied and the effect of a void is to generate a stress concentration at the void tip. The effect of a flaw on the stress is usually described (e.g., Hertzberg, 1976; and Knott, 1973) as:

$$\sigma_{max} = \sigma_{avg}(1 + \sqrt{\pi a}) \qquad (17)$$

σ_{avg} is the average stress, 2a is the length of the flaw, and k is a constant. The expression assumes a flaw with sharp edges. Equation 17 assumes that the radius of curvature at the flaw tip is independent of the flaw size. Another aspect to consider is the size of the hematite grains should have an effect on the flaw size in Equation 17. Although the voids were considered spherical in the previous calculations, at the microscopic level they present irregularities (gaps between individual hematite particles) that fulfill the requirement to be considered as a flaw. Hence, the tensile stress experienced by the center of the pellet (Equation 16) has to be corrected for the existence of flaws:

$$P_c = \frac{\pi^2 d^2 \sigma_c}{8(1 + k\sqrt{\pi a})} \qquad (18)$$

For instance, a small pellet that does not have a void in the center might be stronger than a larger pellet with a flaw.

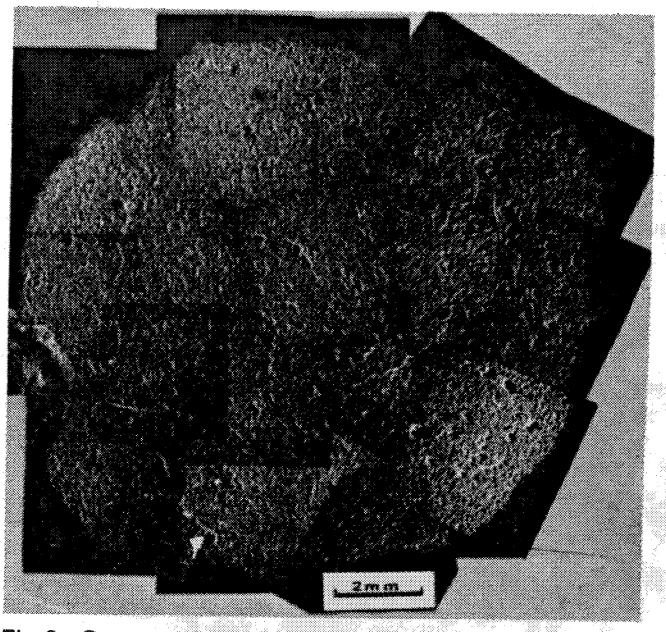

Fig. 8—Cross-section of pellet showing voids

Improved Testing Techniques

Preliminary Considerations

Figure 7 shows the main problem in mechanical testing of pellets—the scatter in the results. As the strength requirements for the pellets become more rigorous, a greater and greater number of individual tests is required. In some situations it exceeds 100.

In the first part a mathematical analysis was introduced that normalizes pellet strength with respect to the cross-sectional area. However, the scatter around the least-squares fit is still very large, leading the authors to investigate alternative testing techniques.

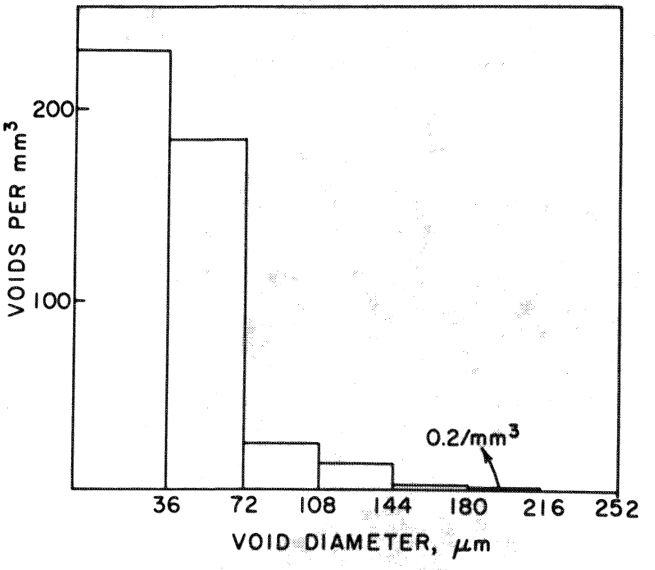

Fig. 9—Density of voids versus diameter assuming spherical voids, using Spektor's technique

Accordingly, two systems were developed. The first consists of inserting the pellet between steel spheres. The second consists of a steel cylinder and piston where a number of pellets are loaded and simultaneously crushed. Three tests are sufficient to characterize the mechanical strength of the pellets in the cylinder-and-piston test. It is hoped that the second testing procedure will be adopted by industry after appropriate parameter optimization.

Six-Spheres Test

The conventional test of compressing the pellet between parallel flat platens does not simulate very well the environment actually encountered by the pellet. Each pellet is surrounded by similar pellets that exert a pressure on it whose magnitude is dependent on the height of the pile, among other parameters. The most compact ways in which spheres pack themselves are close-packed hexagonal and face-centered cubic. The closest-packed planes are stacked in sequences AB AB and ABC ABC, respectively. The latter stacking sequence was chosen to represent the packing of pellets.

Two testing platens were machined and three steel spheres were inserted in each. The pellets were placed between the two platens (Fig. 10). The spheres on the top platen were not placed vertically above the ones in the bottom layer in order to better simulate the ABC stacking sequence, where the pellet corresponds to B.

The results of tests conducted on about 70 pellets are shown in Fig. 11. The load of fracture is plotted against the cross-sectional area. Both the slope of the least-square line and its intercept with the load axis are higher than those of the conventional flat-platen test (Fig. 7). Nevertheless, there seems to be no improvement in the scatter of the fracture load over the latter test.

Hence, the increase in the number of contact points from two to six, with a more uniform concentration of stress, did not improve the results. This showed that the variation in pellet strength was not connected to irregularities in the contact regions, confirming the mathematical analysis and observations presented earlier. One conclusion that can be drawn from the six-spheres test is that the strength of the pellet is somewhat higher (~30%) in the actual environment than between flat platens.

Most of the tests using the six-spheres system were continued beyond the first crack propagating through the pellet. Actually, the first crack did not propagate through its center. Failure had a more progressive, continuous response, and the pellet retained a considerable load-bearing ability after the first crack

propagated. The cracks produced "scaling" or "peeling off" of successive layers of the pellet. For this reason, the tests were continued until complete disintegration of the pellet.

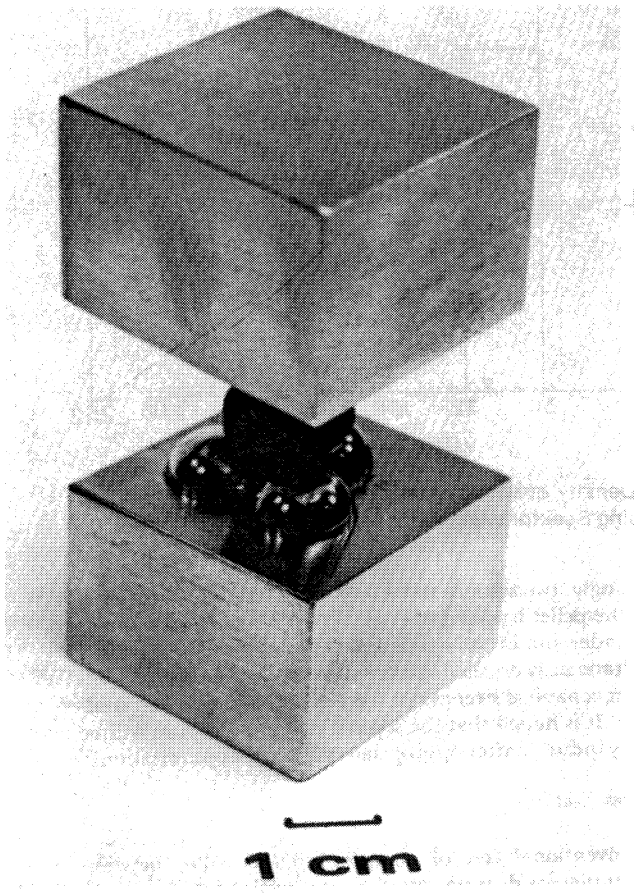

Fig. 10—Improved set-up for testing mechanical strength of pellets consisting of three steel spheres on each plate; pellet is placed between plates so that spheres are not in direct superposition

Figure 12 shows a typical fractured pellet. The load versus extension curves are shown in Fig. 13. Since the fracture load — first peak in load versus extension curve — varied so much, it was thought that the energy absorbed in the crushing process might be a better measure of the strength of the pellet. This energy is given by the area under the load versus extension curves in Fig. 13. It can be readily seen that the units are N.m.

Three plots are given in Fig. 13 and show the different responses exhibited by pellets. For type A pellets, the fracture load is higher than the remainder of the curve. For type B pellets, the pellet recovers its strength after the first drop and the load reaches a level roughly equal to the initial fracture load. Type C pellets, on the other hand, exhibit a higher strength after some deformation than at the first fracture. These three responses show that the fracture load is not representative of the load-bearing ability of the pellets.

Figure 14 shows the energy absorbed in the crushing process as a function of pellet cross-sectional area. No improvement is obtained over the plots of Figs. 7 and 11. The scatter in the data is still very substantial.

In spite of the fact that the six-spheres test exhibits the same limitations than the flat-platen test, it is fundamentally more significant, since it simulates better the loading environment actually encountered by the pellets.

Cylinder-and-Piston Test

The realization that the individual variation in pellet strength was unavoidable due to existing internal flaws and size differences led to the development testing procedure using a thick-walled cylinder and a loosely fitted piston (Fig. 15.).

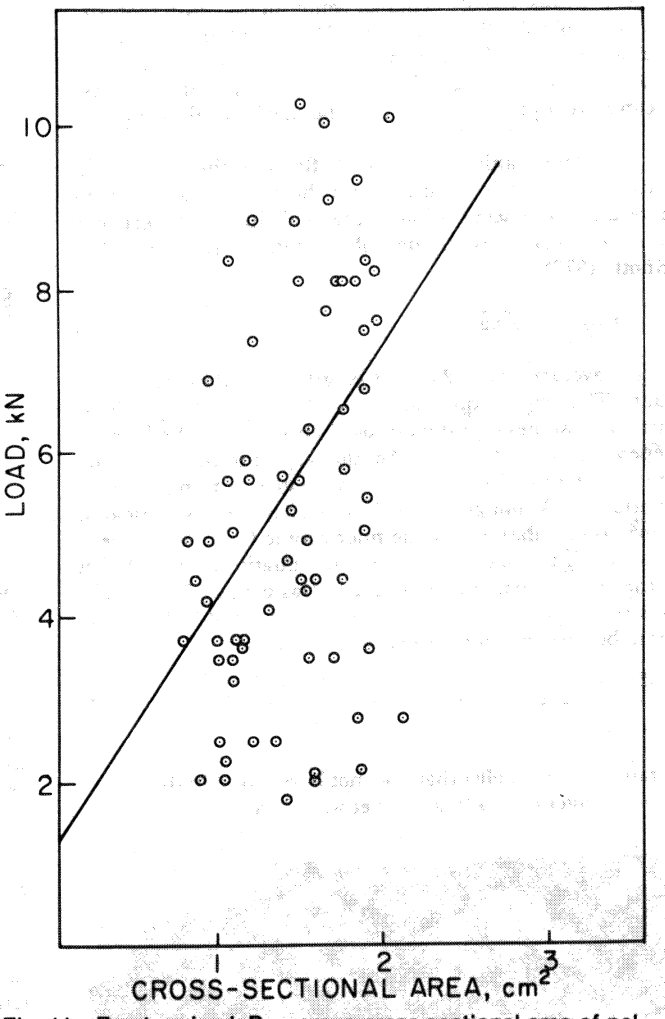

Fig. 11—Fracture load, P_C, versus cross-sectional area of pellets, using improved six-spheres test; straight line represents least-square fit

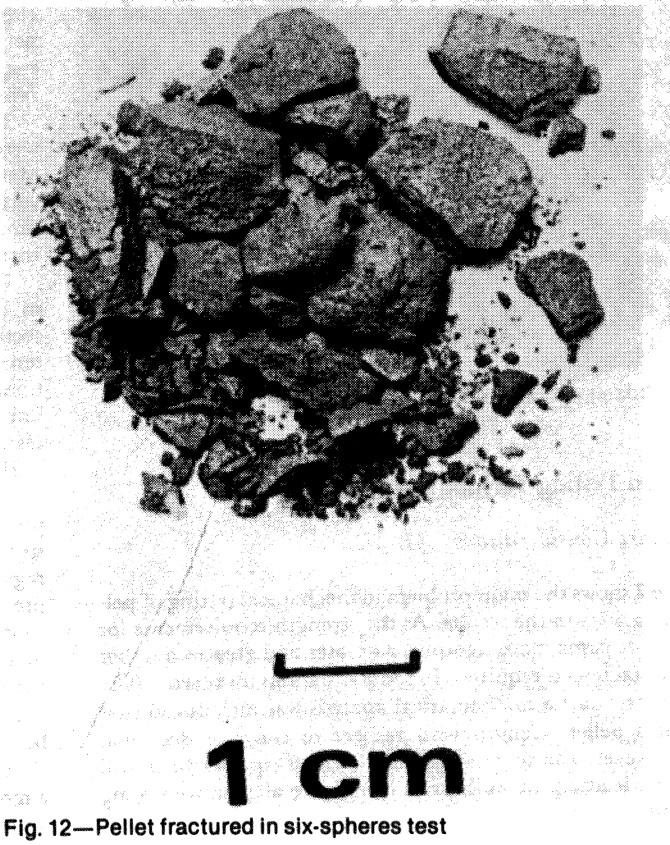

Fig. 12—Pellet fractured in six-spheres test

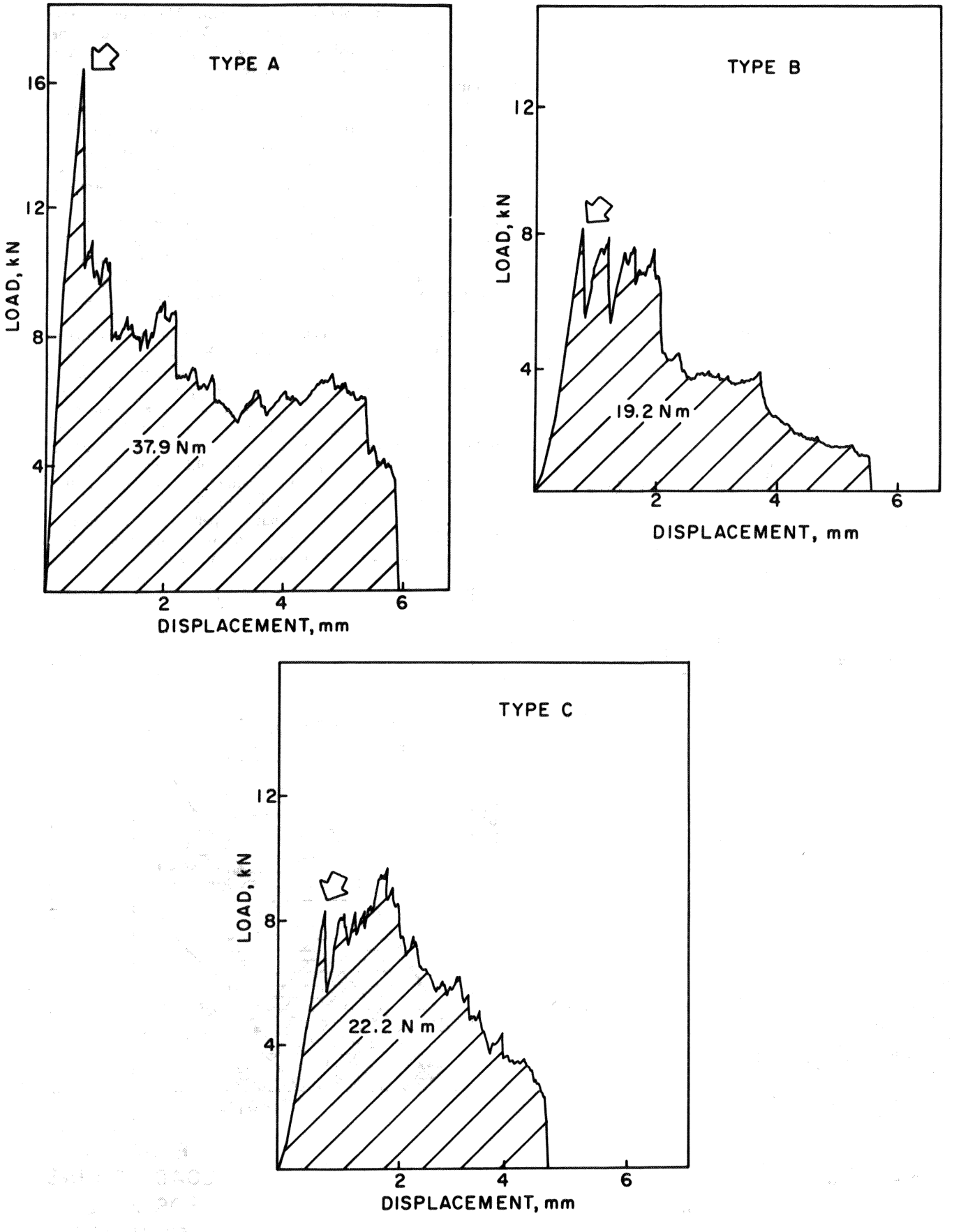

Fig. 13—Load versus displacement curves in six-spheres test. Curves are classified into types A, B, or C depending upon whether the fracture load is higher, equal, or lower than the loads on subsequent compression

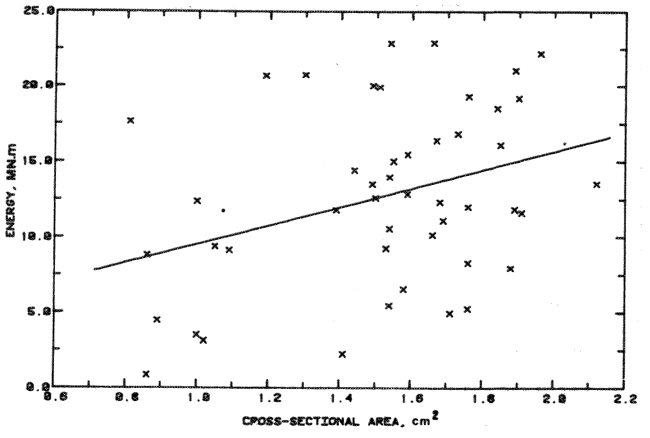

Fig. 14—Energy absorbed in crushing process versus cross-sectional area, using improved six-spheres test; straight line represents least-square fit

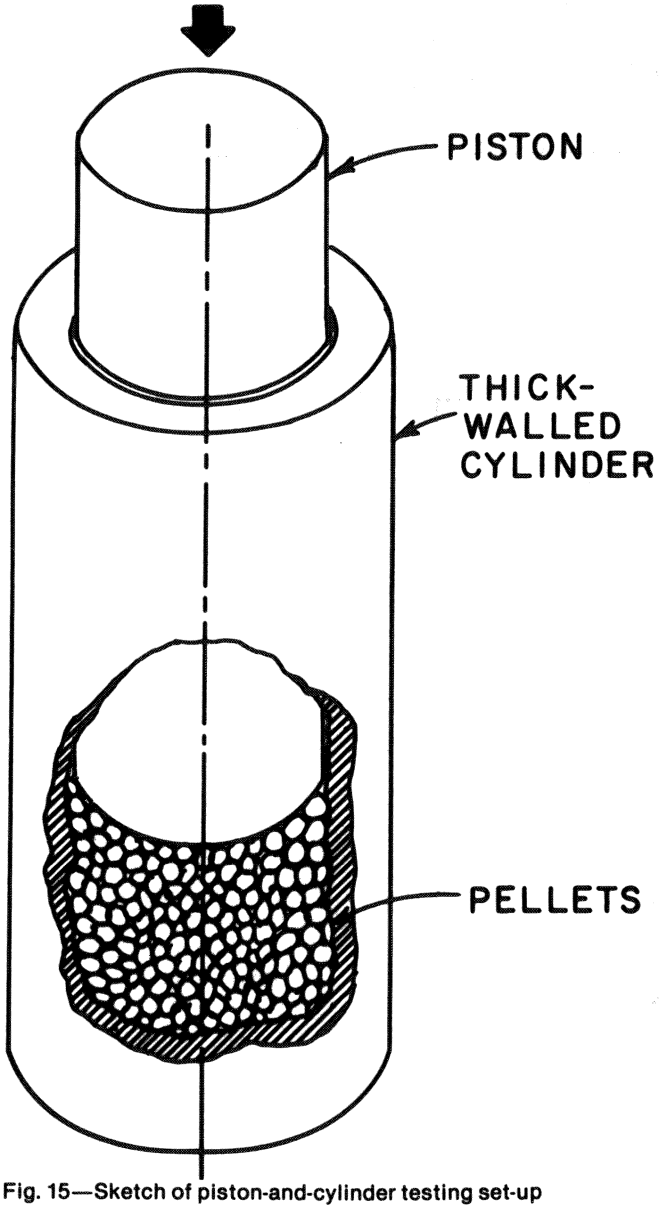

Fig. 15—Sketch of piston-and-cylinder testing set-up

Pellets are loaded into the cylinder up to a standard height. The system used in the present investigation had a height of 305 mm (1 ft), an internal diameter of 63 mm (2.5 in.) and the pellets were loaded up to a height of 127 mm (5 in.). The system was compressed in a Baldwin compression testing machine at a velocity of 20 mm/min (0.8 in. per min). The extension was monitored by means of a transducer (LVDT) attached to the top portion. The load and extension were fed into an X-Y recorder. The total duration of a test was of approximately 15 minutes.

The main goal in developing this test was to obtain a parameter that satisfactorily described the compressive strength of a batch of pellets in a simple and readily reproduceable test. Figure 16 shows the types of stress versus strain plots to be expected of batches of pellets with different strength. The stress is calculated by dividing the load by the cross-sectional area of the piston. The strain is obtained by dividing the extension dL by the initial length of the pellet load. As the piston descends, the pellets are crushed and a progressively higher load is required. Since a large number of pellets is involved it was thought that the individual fracture events would average out, resulting in a smooth curve.

The stress versus strain curve should asymptotically approach the elastic loading line for totally crushed pellets. The total strain can be calculated and one assumes that the totally crushed pellets have the theoretical density of the pellet, 3.83 t/m^3 (3.83 g/cm^3) as a first approximation. The apparent density of the pellets (weight of a certain quantity divided by its volume) was found to be 1.95 t/m^3 (1.95 g/cm^3). Dividing this value by the theoretical specific weight is 0.5. Hence, complete crushing should be achieved at a strain of 0.5. At a strain of 0.5 the curves should approach the line for the elastic modulus of hematite. It should be noted that the pellets used in this test should be closely sized, because the initial packing of the pellets will subsequently affect the measured strain values.

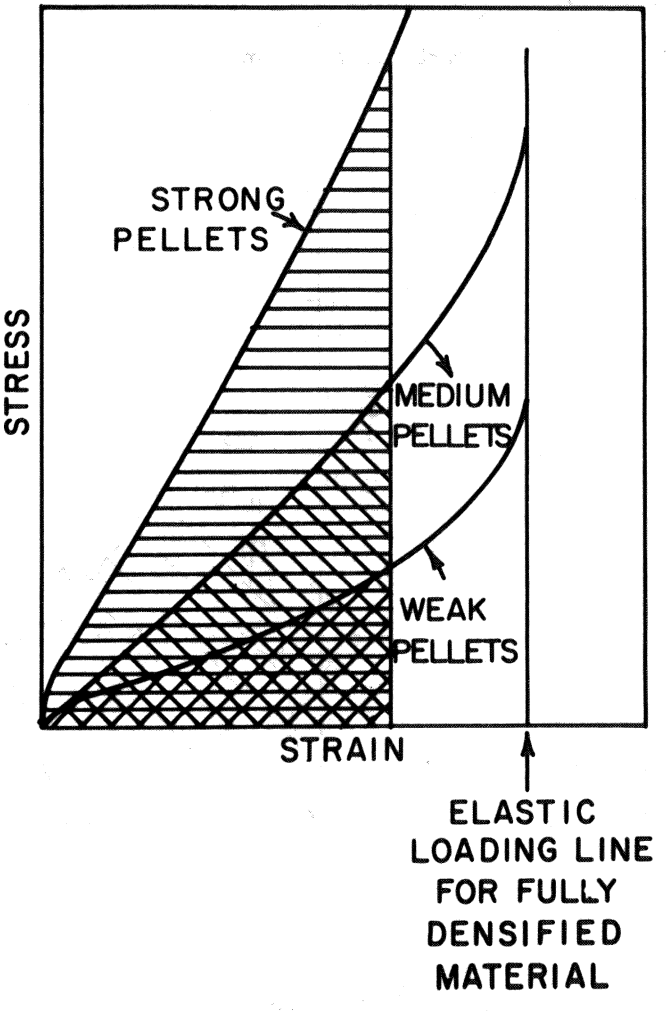

Fig. 16—Schematic representation of stress vs strain curves for strong, medium, and weak pellets using improved testing procedure (piston-and-cylinder)

Since this value of strain is only obtained at very high values of stress, for stronger pellets, a certain amount of strain was arbitrarily chosen. The area under the different curves expresses the energy required to crush the pellets to the arbitrarily chosen strain and is a satisfactory measure of the compressive strength of pellets.

The application of the above concepts to actual pellets is shown in Fig. 17. Four individual tests are shown in the figure and they are in fair agreement. The energies absorbed up to a strain of 0.25 were measured from the area under the curve — the mean is 3128 N·m and the standard deviation is 651 N·m. The variation in this parameter from test to test is far lower than that of the individual pellets (either fracture load or energy absorbed). It is thought that such a test, upon appropriate standardization after optimization of the parameters, would provide a simpler and superior description of the pellet compressive strength. Figure 18 shows the percentage of pellets fractured as a function of strain. One can see that the curve is S shaped and that the strain of .5 was set as 100% fractured. Actually, a distinction should be traced between fractured and crushed — 100% fractured should correspond to a strain slightly lower than 100% crushed.

Nevertheless, the results of Fig. 18 show that the stress level used in the test is sufficient to produce fracture of a considerable percentage of the pellets; the five tests grouped around 80% fractured correspond to the plots of Fig. 17.

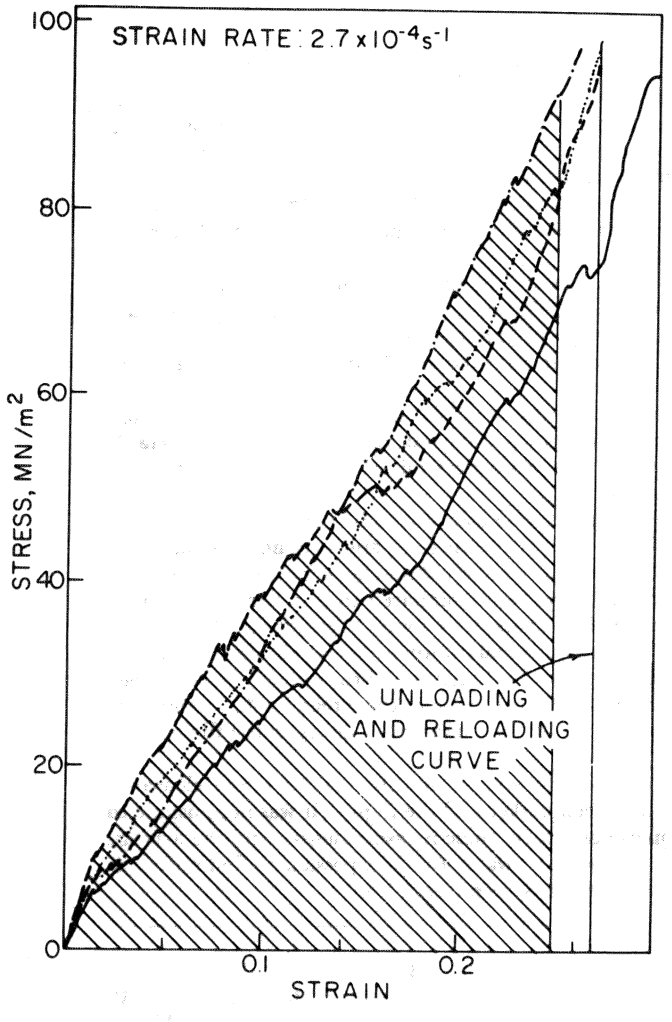

Fig. 17—Stress versus strain curves for four different tests using the same pellet height of 130 mm (5 in.) inside cylinder.

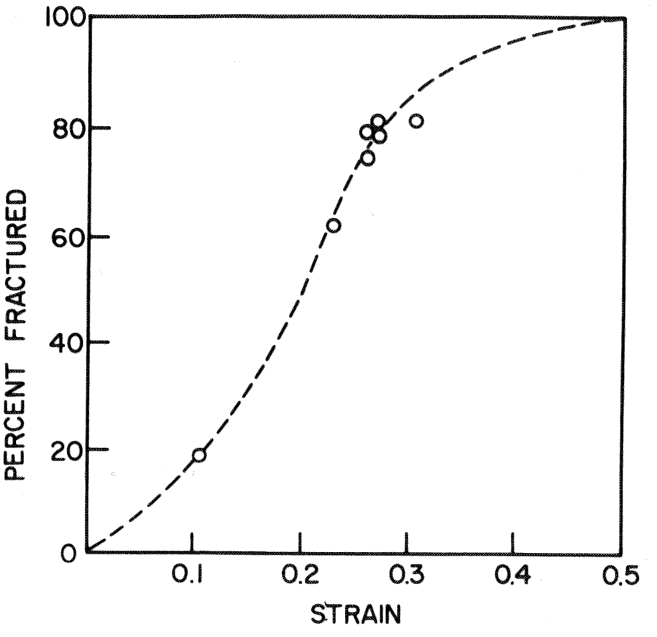

Fig. 18—Percentage of pellets fractured versus strain in piston-and-cylinder test

Conclusion

- A mathematical analysis conducted on a sphere compressed between parallel plates shows that the pellet strength increases linearly with cross-sectional area if failure is produced by a tensile crack starting at the center.
- Observation of the fracture morphology by optical and scanning electron microscopy identifies the main fracture regime as being one induced by tensile stresses.
- In spite of the considerable scatter in the data, the pellet strength is shown to be proportional to the square of the diameter (in the conventional test between flat and parallel platens), in accord with mathematical analysis.
- It is shown that there is a substantial amount of voids in the pellets with diameter up to 0.3 mm (.001 in.). These voids are shown to be responsible for the large variation in fracture strength between individual pellets, because they act as stress-concentration sites, weakening the pellet.
- Two improved testing procedures are proposed. The first consists of compressing a pellet between platens containing three steel spheres in contact each. This set up simulates much more realistically the environment actually encountered by the pellet (pellet among pellets) and yields fracture loads higher than the conventional test. An additional advantage is that the fracture process is progressive and not catastrophic, as in the conventional test. However, the scatter in the data remains essentially unchanged.

The second test consists of a set up with a thick-walled cylinder into which a piston slides. A large number of pellets are crushed in a single test, yielding a stress versus strain curve that describes satisfactorily the compressive strength of the pellet. ■

Acknowledgments

Professor D.W. Fuerstenau (University of California at Berkeley) suggested this research program; in this sense his contribution was invaluable. Discussions with Dr. K.I. Oravecz (New Mexico Institute of Mining and Technology) clarified many obscure points; his help in setting up the experiments is greatly acknowledged. Part of the experimental work was conducted by S. Patel, K. Couch, and S.-H. Pan. This research was partially supported by National Science Foundation Grant No. DMR-797-102.

References

deHoff, R., and Rhines, F.N., 1968, eds., *Quantitative Microscopy,* McGraw-Hill, New York, p. 183.

Dieter, G., 1976, *Mechanical Metallurgy,* McGraw-Hill, New York, 2nd edition, p. 604.

Hertz, H., 1896, *Hertz's Miscellaneous Papers,* MacMillan, London.

Hertzberg, R.W., 1976, *Deformation and Fracture Mechanics of Engineering Materials,* J. Wiley, New York.

Jaeger, J.C., and Cook, N.G.W., 1979, *Fundamentals of Rock Mechanics,* 3rd edition, Chapman and Hall, London, p. 171.

Kapur, P.C., and Fuerstenau, D.W., 1967, *J. Am. Cer. Soc.,* Vol. 50, p. 14.

Knot, J.F., 1973, *Fundamentals of Fracture Mechanics,* J. Wiley (Halsted Press), New York.

McGannon, H.E., 1971, ed., *The Making, Shaping, and Treating of Steel,* US Steel, 9th edition, p. 891.

Popov, E.P., *Mechanics of Materials,* Prentice-Hall, Englewood Cliff, NJ, 1976, p. 298.

Sastry, K.V.S., 1974, *Agglomeration 77,* AIME, New York.

Sternberg, E., and Rosenthal, F., 1952, *J. Appl. Mech.,* Vol. 74, p. 413.

Timoshenko, S., 1934, *Theory of Elasticity,* first edition, McGraw-Hill, New York, p. 104.

TECHNICAL NOTE

Performance of CMI EB-36 Centrifuges

W.T. Walter and M.R. Meyer

Introduction

A great deal is known, in a qualitative sense, about the performance of CMI EB-36 centrifuges. The manufacturer can give reliable guidance for the proper operation of its centrifuges and can give general estimates of expected product moisture and recovery.

Quantitative estimates of the effects of changes in the various operating parameters are more difficult to find. The engineer faced with designing a preparation plant may be without the specific data needed to make decisions. For example, to obtain optimum product moisture when drying 9.5 mm × 595 μm (0.4 in. × 28 mesh) coal the centrifuge manufacturer recommends having no more than 5% -595 μm (-28 mesh) material in the centrifuge feed. They know that more -595 μm (-28 mesh) material in the feed will cause higher product moistures, but they usually cannot quantify the increased moisture or describe the shape of the product moisture versus -595 μm (-28 mesh) in the feed curve.

This study was conceived to provide quantitative information on the EB-36 centrifuges, focusing on product moisture, recovery, and size degradation. All of the centrifuges tested were Model EB-36 dryers from Centrifugal and Mechanical Industries Inc. (CMI), with feeds in the nominal 9.5 mm × 595 μm (0.4 in. × 28 mesh) range. These are typical centrifugal dryers in this application, and many were available for testing.

Testing

Eighteen different CMI EB-36 centrifuges were tested at five different preparation plants. The coals tested included Pittsburgh No. 8 seam from northern West Virginia, Lower Kittaning seam from southwestern Pennsylvania, a subbituminous coal from New Mexico, and a mixture of Pocahontas 3, Pocahontas 6 and Beckley seam from southern West Virginia.

During each test, samples were taken at regular intervals of the feed, product, and effluent for each machine. The standard test consisted of 16 sample cuts over four hours. Each machine was tested on at least two separate occasions. In addition to the material samples, effluent flow measurements were taken from each effluent pipe. The flows were measured in duplicate using the "bucket and stopwatch" technique. If the duplicates did not agree to within ±10% the measurements were repeated. The effluent flows were measured for each EB-36 at least three times during each test. The flow rates for each effluent pipe of a machine were averaged and then summed to give the average effluent flow for each centrifuge.

For all of the material samples the following were determined:

- Air-dry and total moisture or percent solids, whichever was appropriate.
- Screen analysis at 6.35 mm (0.25 in.), 2.38 mm (8 mesh), 1.19 mm (14 mesh), 595 μm (28 mesh), 250 μm (60 mesh), 149 μm (100 mesh), 74 μm (200 mesh), and 44 μm (325 mesh). Some of the samples were also screened at 9.5 mm (0.4 in.) and 12.7 mm (0.5 in.).
- Ash and sulfur on the solids. In many cases the water from the effluent samples was analyzed for pH and hardness. Hardgrove grindabilities were determined on the centrifuge feed samples for each test.

Surface moistures were assumed to be equal to air-dry moistures for eastern coals (44 of the tests) and were not calculated for western coals (five of the tests). As a check for the eastern coals, the air-dry moistures were compared to (total moisture minus equilibrium moisture) and were found to match closely.

At each plant additional information was obtained on the individual EB-36s. This included size of the opening in the screen basket; material of construction of the screen basket; number of hours on the screen basket; number of hours on the flights; and type of cone cap.

Two pieces of information not obtained were the clearance between the screen basket and the flights (It was not possible to disrupt operations to get these measurements), and the average life of screen baskets (It was not usually possible to find meaningful records of average screen basket life).

W.T. Walter, member SME, is chief reserve evaluation engineer, and **M.R. Meyer,** member SME, is a senior testing engineer, both with Consolidation Coal Co., Pittsburgh, PA.

SME preprint 82-80. SME-AIME Annual Meeting, Dallas, TX, Feb. 1982. Manuscript Jan. 1982.